

Fluorescent Compounds

Unexpected Photoluminescence of Fluorinated Naphthalene Diimides

Subashani Maniam, Rosalind P. Cox, Steven J. Langford,* and Toby D. M. Bell*[a]

Abstract: Two new amino core-substituted naphthalene diimides (cNDIs) bearing fluorinated side chains have been synthesised. Steady-state and time-resolved fluorescence spectroscopy reveals unprecedented optical properties for the cNDIs with high quantum yields of ~0.8 and fluorescence lifetimes of ~13 ns in a range of solvents. These properties are apparent at the level of single molecules, where the compounds also show exceptional photostability under pulsed-laser excitation. Photon emission is remarkably con-

sistent with very few long timescale (millisecond or longer) interruptions with molecules regularly undergoing $>10^7$ cycles of excitation and emission. Intermittencies owing to triplet-state formation occur on a sub-millisecond timescale with a low yield of 1–2%, indicating that the presence of the fluorine atoms does not lead to a significant triplet yield through the heavy-atom effect. These properties make the compounds excellent candidates for single-molecule labelling applications.

Introduction

Informed design of new compounds derived from an optically active parent with the goal of obtaining improved spectroscopic properties is a long-standing and proven approach. Fluorination has proved to be one successful strategy to alter the energy levels of molecular orbitals,^[1,2] tune molecular packing,^[3,4] and increase solubility within a family.^[5,6] This methodology has been used as part of the molecular design strategy for application in field-effect transistors (OFETs), dye-sensitised solar cells (DSSCs) and photovoltaics (PVs).^[7–9] One drawback, however, is that luminescent properties are usually highly compromised in the presence of fluorine atoms due to the heavy-atom effect (HAE). This effect is where the presence of 'heavy' atoms (e.g., substitution of hydrogen atoms by halogen atoms) promotes singlet–triplet conversion by intersystem crossing, thereby reducing the fluorescence quantum yield and the excited-state lifetime of a molecule.^[10–12] In addition to the HAE, the high electronegativity of fluorine atoms can further decrease fluorescence quantum yield by withdrawing electron density away from the conjugated system of a chromophore.^[13] However, some recent investigations have shown that halogens can have a positive effect on luminescence properties. For example, an increase in fluorescence quantum

yield has been observed for a series of halogenated squaraine dyes.^[14] This investigation suggests that there is a redistribution of electron density of the halogen atom from its HOMO to the LUMO energy level of the conjugated system, therefore strengthening the π -system upon excitation. Increases in quantum yields and fluorescence lifetimes for series of fluorinated boron-dipyrromethenes (BODIPYs) dyes has also been demonstrated, as have the tunability of fluorescence in stilbene-based molecules through different halogen- and hydrogen-bonding interactions.^[15,16] Further investigations have focused on the effect of halogenation on the solid-state fluorescence and electroluminescence properties of oligo(phenylene vinylene).^[17] In all of these examples, however, halogen atoms, and particularly fluorine atoms, are directly attached to a conjugated system.

In our efforts to develop naphthalene diimides (NDIs) as versatile aromatic compounds and realise some of their enormous potential, we have developed synthetic strategies that have led to the preparation of NDIs in single-molecule and biophysical applications,^[18,19] as sensors,^[20,21] and in supramolecular architectures.^[22,23] The potential for a chromophore to be observed by fluorescence at a single-molecule level relies strongly on its 'molecular brightness', which in its simplest form can be approximated by the product of molar absorption coefficient and fluorescence quantum yield.^[24,25] Core-substituted NDIs (cNDIs) perform quite well on the quantum yield side of the equation, with a number of reported compounds displaying quantum yields of $0.3 < \Phi_f < 0.5$.^[26,27] On the absorption side of molecular brightness, the issue with cNDIs is their relatively low molar absorption coefficients, which typically fall in the range of $10\,000\text{--}20\,000\text{ cm}^{-1}\text{ M}^{-1}$.^[21,27] Thus, the cNDIs reported so far do not have the molecular brightness of the larger rylene imide derivatives or other fluorophore families such as the cyanines and rhodamines, for example. cNDIs have, however, been successfully imaged as single molecules^[18] and are

[a] Dr. S. Maniam,[†] R. P. Cox,[†] Prof. S. J. Langford, Dr. T. D. M. Bell
School of Chemistry
Monash University
Wellington Rd, Clayton 3800, Victoria (Australia)
Fax: (+613) 9905 4597
E-mail: steven.langford@monash.edu
toby.bell@monash.edu

[†] Both authors contributed equally to this work.

Supporting information for this article is available on the WWW under <http://dx.doi.org/10.1002/chem.201405876>.

good candidates in single-molecule labelling applications as they undergo relatively few interruptions, or 'blinks' to their fluorescence emission. This, plus their tunable optical properties and ready functionalisation, mean interest in cNDIs remains high.

Continued progress in the application of cNDIs^[27,28] requires further development of the synthetic methodologies that access systems with novel properties. Fluorinated moieties are easily introduced at the N-imide positions of NDIs,^[29–33] however, thus far, there are few examples of fluorinated cNDIs.^[34,35] One successful approach has been to append fluoroalkyl moieties directly onto the core, which causes strong negative spectroscopic changes.^[17] As part of our continuing development of cNDIs with new and improved optical properties, we have synthesised new cNDIs **4** and **5** bearing fluorinated alkyl side groups, which are typically used to impart solubility. We observed an unusual increase in the fluorescence quantum yield and lifetime, to around 0.8 and 13 ns, respectively, in both cNDIs **4** and **5** with only small variation with solvent. This is carried through to the single-molecule level, where molecules of **4** show a significant increase in molecular brightness compared with previous cNDIs, exceptional photostability, and almost uninterrupted photon emission intensity.

Results and Discussion

Compounds **4** and **5** (Figure 1a), bearing non-fluorinated and fluorinated alkyl substituents at the N-imides, respectively, and core di-substituted with amino-methylene-perfluoroalkyl groups, were synthesised by using Hartwig–Buchwald coupling conditions (Scheme 1). This core-substitution synthetic methodology is not commonly utilised for NDIs;^[28] however, was necessary as the known electron-withdrawing nature of the fluorinated moiety decreased the nucleophilicity of the amine. Full synthetic characterisation of **4** and **5** can be found in the Supporting Information along with synthetic details for the intermediate for **4** (Figures S1–S11 in the Supporting Information).

Deep-red crystals of **5** suitable for X-ray analysis^[36] were grown from CHCl₃ solution and the resultant structure is shown in Figure 1b. Single-crystal analysis of compound **5** shows that it is planar along the NDI core. Neighbouring molecules of **5** display a canted vertical stacking arrangement (Figure 1b) with the nitrogen atoms of the N-imide centrally located along the ring system of the adjacent NDI group. This orientation leads to π – π stabilisation of the NDI ring with the imide nitrogen giving an average plane separation of 3.4 Å. Within the crystal lattice, columns of **5** extend along the crystallographic *a*-axis, whereas in the *b,c*-plane, **5** adopts a step-stacking approach with the neighbouring molecules, an arrangement that maximises the London dispersive forces within the alkyl chains (Figure S12 in the Supporting Information).

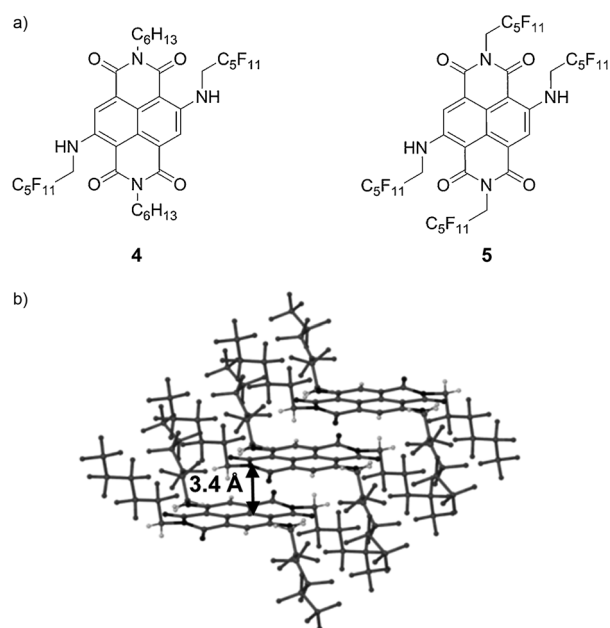
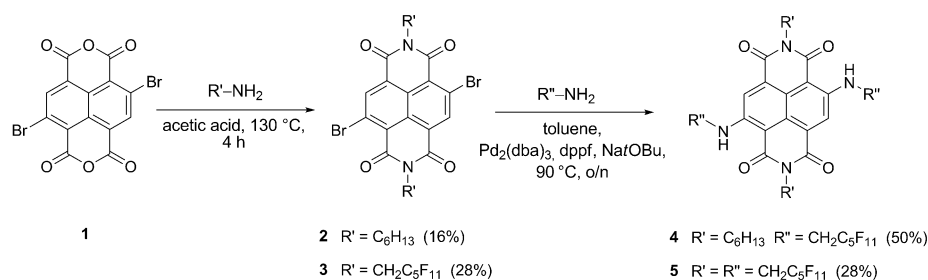


Figure 1. a) Molecular structures of **4** and **5**, and b) X-ray crystallographic structure of **5** showing canted vertical stacking.



Scheme 1. Synthesis of compounds **4** and **5**. dba = dibenzylidenacetone; dppf = 1,1'-bis(diphenylphosphine)ferrocene.

Figure 2 shows the normalised steady-state absorption and emission spectra of **4** and **5** in a CH₂Cl₂ solution measured at room temperature. The absorption spectra display characteristic bands in the near-UV range, at 350 nm and 370 nm, which are assigned to π – π^* transitions, along with a broad band cen-

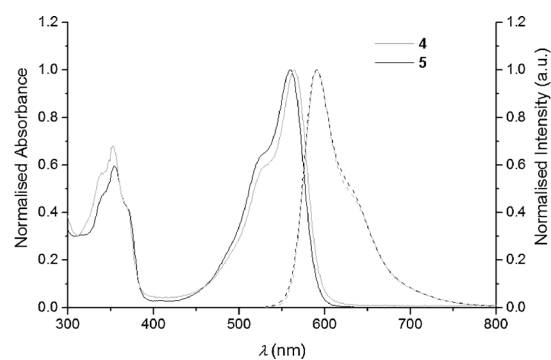


Figure 2. Normalised steady-state absorption and emission spectra ($\lambda_{\text{exc}} = 520\text{ nm}$) of **4** and **5** in CH₂Cl₂ ($1 \times 10^{-5}\text{ M}$).

tered at 560–565 nm, attributed to an $n-\pi^*$ transition. The molar absorption coefficients of **4** and **5** in CH_2Cl_2 are determined to be 15400 and $11500 \text{ M}^{-1} \text{ cm}^{-1}$, respectively (Figure S13 in the Supporting Information) and these spectral features are consistent with previously reported di-amino-substituted NDIs.^[14,20,37–40] Spectra are very similar for both compounds, indicating that the nature of the imide-substituted group has only a minimal effect on the optical properties observed.

Interestingly, emission spectra for both compounds are centered at 590 nm with favourably high fluorescence quantum yields (Φ_f) of 0.85 and 0.75 for **4** and **5**, respectively, in CH_2Cl_2 . The emission maximum of **4** redshifts from 570 nm in *n*-hexane to 594 nm in benzonitrile (PhCN) and the emission maximum of **5** shows a similar trend (see Table 1, and Figures S14 and S15 in the Supporting Information). This observation is likely due to the symmetry of the molecules, which bal-

Table 1. Steady-state and time-resolved optical data for **4** and **5** in various solvents.

Solvent	$\lambda_{\text{max(abs)}}$ [nm]		$\lambda_{\text{max(em)}}$ [nm]		Φ_f		τ_{flu} [ns]	
	4	5	4	5	4	5	4	5
<i>n</i> -hexane	550	555	570	574	$0.89 \pm 0.02^{\text{[a]}}$	0.83 ± 0.03	13.8 ± 0.2	13.8 ± 0.1
toluene	560	565	587	592	0.85 ± 0.02	0.77 ± 0.03	12.7 ± 0.1	13.0 ± 0.1
CH_2Cl_2	560	565	590	593	0.85 ± 0.03	0.75 ± 0.04	12.9 ± 0.2	12.8 ± 0.2
PhCN	564	569	594	597	0.75 ± 0.04	0.73 ± 0.04	12.3 ± 0.1	12.2 ± 0.1

[a] Errors are ± 1 standard deviation from triplicate measurements.

ances the charge distribution, leading to only a weak dependence on solvent polarity. Table 1 also indicates that both **4** and **5** show high Φ_f values across a range of solvent polarities, from completely non-polar *n*-hexane to the quite polar solvent PhCN. The compounds, however, are not soluble in water, where they aggregate. The highest Φ_f value of 0.89 is achieved with **4** in *n*-hexane and Φ_f remains greater than 0.7 for both **4** and **5** in PhCN. These Φ_f values are significantly higher than those reported thus far for core-substituted NDIs^[27] and encourages the development of water-soluble derivatives with the hope that the high Φ_f carries through into this solvent, thus opening the way for use of these compounds in biological-labelling applications. We have recently synthesised and characterised some water-soluble cNDIs with substituents containing a number of oxygen atoms^[19] and derivatives of **4** with such groups at the imide positions are current targets of ours.

The kinetics of the fluorescence emission of **4** and **5** were explored by using time-correlated single-photon counting (TCSPC). A single exponential decay function adequately described the emission in all solvents for **4** and **5** (Figure S16 in the Supporting Information) with observed fluorescence lifetimes of 12.7 and 12.6 ns, respectively, in CH_2Cl_2 (Figure 3). On the basis of the Φ_f values and observed lifetimes, the radiative lifetimes for **4** and **5** were deduced to be 15.3 and 16.1 ns, respectively, in CH_2Cl_2 . In addition, their non-radiative decay rate constants, k_{nr} were calculated to be $1.3 \times 10^7 \text{ s}^{-1}$ for **4** and $1.8 \times 10^7 \text{ s}^{-1}$ for **5**. This suggests that the Φ_f values for **4** and **5** are

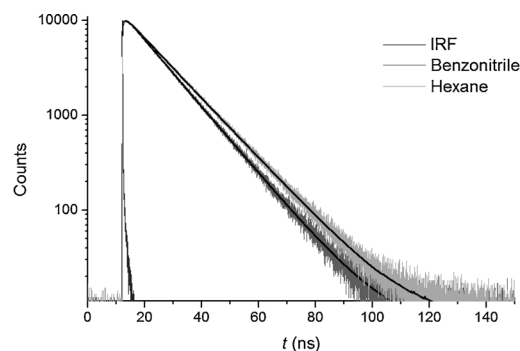


Figure 3. TCSPC decay histograms and fitted single-exponential functions (black) for **4** in *n*-hexane and PhCN. IRF is the instrument response function.

higher than other known NDIs mainly owing to the non-radiative decay being much less efficient than for non-fluorinated cNDIs, presumably due to a decrease in vibrationally mediated non-radiative loss as a result of the F atoms adding mass to the core substituents. k_{nr} increases slightly with polarity (Table S1 in the Supporting Information), thus, the lifetimes marginally decrease; this is consistent with the small reduction in HOMO–LUMO band gap as shown by the redshift of the absorption and emission maxima with increasing polarity. The presence of the F atoms might be expected to increase the rate constant and yield of intersystem crossing to the triplet state through the heavy atom effect, however, the bulk measurements show that this is not occurring to any significant extent. This is likely attributable to the F atoms being located on the substituents and not adjacent to the aromatic core where they would exert more influence. Furthermore, all fluorinated substituents, whether on the core or at the imides, first contain an alkyl carbon ($-\text{CH}_2$) before the fluorinated carbons, heading outwards from the point of attachment.

The HOMO and LUMO energy levels of **4** and **5** were measured by using cyclic voltammetry (Figure 4 and Table S2 in the Supporting Information). Compound **4** displays two well-defined reversible one-electron redox processes, with the first reduction and oxidation $E_{1/2}$ values of -1.19 V and 1.08 V (vs Fc/Fc^+). Thus, for compound **4**, the HOMO energy level is

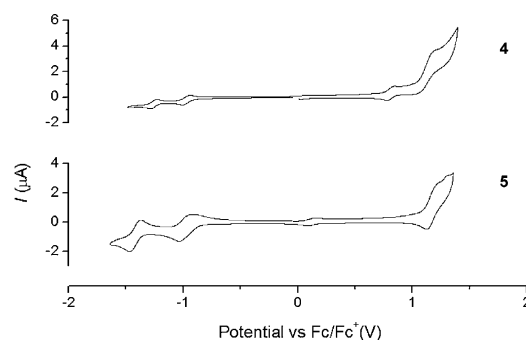


Figure 4. Cyclic voltammograms of **4** and **5** in CH_2Cl_2 (0.5 mM) solutions containing 0.1 M Bu_4NPF_6 as the supporting electrolyte at a scan rate of 100 mVs^{-1} .

–5.88 eV and the LUMO is –3.62 eV. By introducing fluorinated groups at the N-imide positions, compound **5** has deeper HOMO and LUMO energy levels of –5.99 eV and –3.82 eV, respectively. These HOMO–LUMO electrochemical band gaps agree well with the S_1 – S_0 energy difference (optical band gaps) indicated by the spectral maxima of these compounds. The presence of the electron-withdrawing groups has reduced the HOMO–LUMO band gap, from 2.26 eV for compound **4** to 2.17 eV for compound **5**, which is consistent with the slight redshift (~5 nm, 0.05 eV) recorded in the optical spectra.

A detailed investigation of **4** as single molecules was performed to see if its favourable optical properties were carried through to the single-molecule level. **4** was chosen for this analysis as it outperforms **5** in both quantum yield and molar absorption coefficient and is thus expected to show greater molecular brightness. Figure 5a shows a wide-field fluorescence image of **4** embedded in a poly(methyl methacrylate) (PMMA) film. It can be seen that single molecules manifest as bright diffraction-limited point-spread functions when excited with 532 nm light. Under quite gentle illumination conditions (~0.1 kW cm⁻²), the molecules typically showed a signal-to-noise value of ~4.

Single molecules of **4** were also studied by using confocal fluorescence microscopy. 10 × 10 μm areas (Figure 5b) were

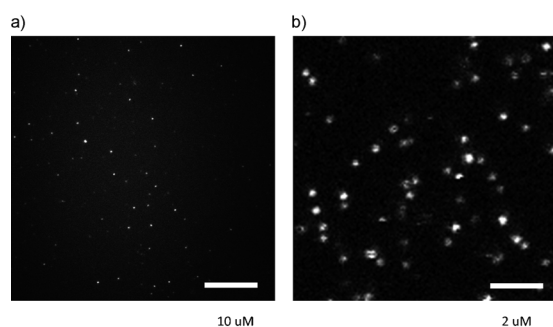


Figure 5. Single molecules of **4** embedded in a PMMA film. a) Wide-field fluorescence microscopy image. Scale bar: 10 μm. Excitation at 532 nm. b) Confocal scan of a 10 × 10 μm area, 1 ms/pixel dwell time. Scale bar: 2 μm. Excitation at 560 nm.

raster scanned to identify single molecules and their time-tagged photon streams and spectral data were collected. In total, emission from 150 individual molecules was studied. Figure 6 shows example emission trajectories of four individual molecules. Most molecules produced intensity traces with little variation in photon count rate other than statistical noise. Encouragingly, single molecules showed little to no blinking and most emitted for longer than 1 min, indicating excellent photostability.

Molecules a and b in Figure 6 show typical trajectories where the emission has a stable count rate before irreversibly photobleaching in a single step. Molecule c displays a clear blinking event at 55 s, which lasts less than 500 ms before partial recovery of intensity that lasts for a further 1.2 s. This is followed by a transition to a long-lived (at least 4 s) dim state of a similar intensity to the blinking event. Long-lived intermitten-

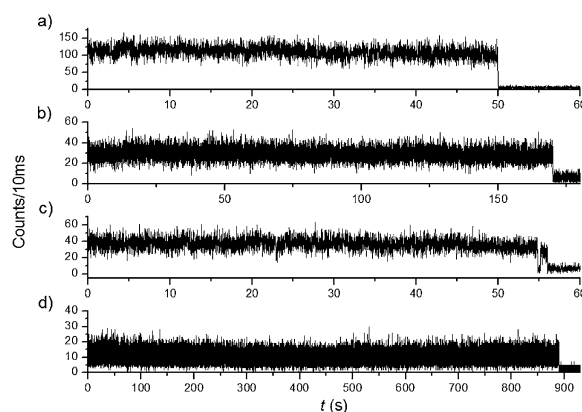


Figure 6. Emission trajectories of four single molecules of **4** in a PMMA film in ambient atmosphere. Excitation at 560 nm.

cies or transitions to dim states were very infrequent and observed in less than 10% of the total single molecules studied. Factoring in the detection efficiency of the single molecule (SM) set-up, where ~5% of emitted photons are detected by the avalanche photodiode (APD), it can be estimated that over 50% of single molecules of **4** emit more than 1×10^7 photons. Some molecules showed remarkable longevity, for example, molecule d emitted an almost continuous stream of photons for longer than 10 min, undergoing more than 1×10^8 excitation–emission cycles before photobleaching.

The fluorescence lifetimes of **4** varied from molecule to molecule over a range from ~6–22 ns, however, they were centred at approximately 13 ns, which is similar to the bulk values measured in solvent. Figure 7 shows an example of lifetimes calculated along the trajectory of a single molecule, an example fluorescence-decay profile, and the lifetime distribution for all molecules analysed. Decay lifetimes were determined from histograms created by binning consecutive amounts of 10 000 photons. Individual molecules showed stable lifetimes—the variation of < 1 ns in the decay lifetime of the molecule in

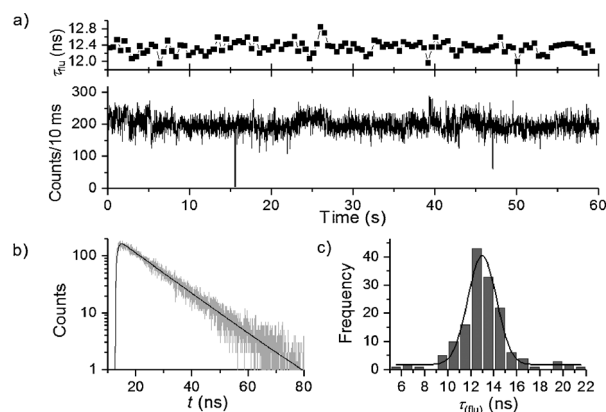


Figure 7. a) Emission trajectory and decay times for a single molecule of **4** embedded in a PMMA film. Lifetimes were calculated from decay profiles created by binning successive packets of 10 000 photons. b) A typical decay profile and fit for **4**. c) A fluorescence lifetime distribution of all the single molecules analysed.

Figure 7 is typical—making assignment of each molecule into 1 ns bins for the histogram straightforward.

Emission spectra were measured for single molecules embedded in PMMA. Example emission spectra are shown in Figure 8, with single molecules emitting sufficient photons for successive spectra to be taken every second. The fluorescence is very stable, with the emission maxima centred at 578 nm and varying only ± 3 nm across 60 spectra. This molecule is

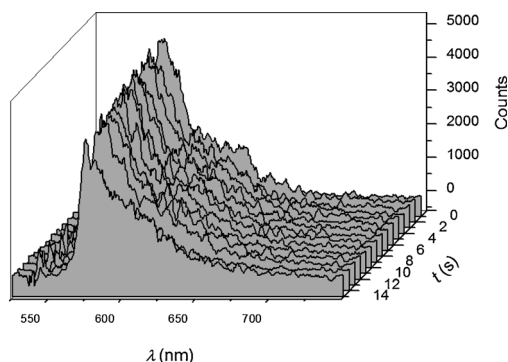


Figure 8. Emission spectra from a single molecule of **4** embedded in a PMMA film. Successive spectra were recorded every second. Excitation at 532 nm.

representative of the molecules studied, with minimal spectral shifts across the time observed. Emission maxima varied slightly between molecules, ranging between 576–581 nm. This is consistent with the emission maxima measured in the bulk properties.

Interruptions or ‘blinks’ to a single molecule’s photon emission can occur through a variety of mechanisms. Inspection of single-molecule trajectories of **4** reveals that blinks of sufficient duration to be visible in the trajectories when binned in 10 ms bins (e.g., the event at 14 s in Figure 9a, which lasts 20 ms) are exceedingly rare and when they do occur are not particularly long-lasting. Long duration interruptions to photon emission

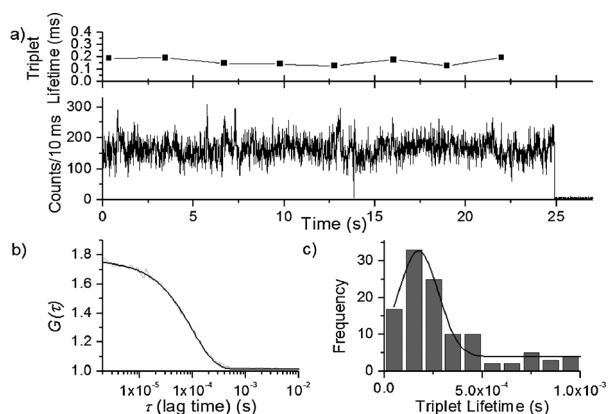


Figure 9. a) Emission trajectory and the calculated triplet lifetime for a single molecule of **4** embedded in a PMMA film. Triplet lifetimes were calculated from autocorrelation curves created by binning successive packets of 50 000 photons. b) Autocorrelation curve and fit for **4** in ambient atmosphere. c) The triplet lifetime distribution of all the single molecules analysed.

are often observed in single molecules and can arise from mechanisms such as electron trapping and oxidation.^[41,42] NDI **4** appears to not suffer any appreciable amount of these blinks and single molecules of **4** emit an uninterrupted and reliable stream of photons. Another intrinsic blinking mechanism available to many fluorophores is triplet formation. Triplet states are usually much shorter lived (microseconds), especially in ambient conditions where collision with oxygen will return the molecule to its ground state whereupon emission can resume. Triplet formation does not present a significant problem when measuring the fluorescence of a compound under bulk concentrations, where a proportion of triplet formation will result in the same proportion decrease in the fluorescent output. However, when studying fluorescent single molecules, the lifetime of the triplet state will have an effect on the photon efficiency. Whereas the triplet yield remains the same, the overall fluorescence intensity over time will be lower as the molecule will not be excited for the duration of the ‘off’ period. When triplet lifetimes are too short to be seen by simple intensity binning, their presence can be revealed by using autocorrelation analysis of the emission intensity from a single molecule.

Autocorrelation functions were generated for the single molecules studied. Figure 9 shows an example molecule emission trajectory with an autocorrelation curve and fit. Intensity autocorrelation functions were generated by calculating the correlation of photon output, I , at any given time, t , with the photon output at a time $(t + \tau)$, shifted by the lag time τ , by using Equation (1):

$$G(\tau) = \frac{\langle \delta I(\tau) \delta I(t + \tau) \rangle}{\langle I \rangle^2} \quad (1)$$

Autocorrelation traces were fit by an exponential decay function, $G(\tau) = A_{AC} \exp[-t/\tau_{AC}]$ with the decay time, τ_{AC} , and the pre-exponential factor, A_{AC} , used to determine ‘on’ and ‘off’ times from Equations (2) and (3):

$$\frac{1}{\tau_{AC}} = \frac{1}{\tau_{off}} + \frac{1}{\tau_{on}} \quad (2)$$

$$A_{AC} \approx \frac{\tau_{off}}{\tau_{on}} \quad (3)$$

These equations are based on the analysis by Weston et al.^[43] and are applicable to a two-state system where the intensity of one state approaches zero, that is, ‘on–off’ behaviour such as that generated by a single fluorescent molecule undergoing triplet-state excursions. For the molecule in Figure 9, τ_{AC} is 97 μ s and A_{AC} is 0.750, yielding a triplet lifetime (τ_{off}) of 170 μ s and τ_{on} of 226 μ s. The triplet yield, or yield of intersystem crossing (ISC), can be calculated by using Equation (4):

$$\phi_{ISC} = \frac{\phi_f \phi_{det}}{\tau_{on} I_f} \quad (4)$$

where Φ_{det} is the detection efficiency ($\sim 5\%$) and I_f is the emission intensity in counts per second (for this molecule,

~ 15000 counts s^{-1}); thus, Φ_{ISC} is 1.2%. The triplet lifetime was measured as a function of time from autocorrelation curves created by binning successive packets of 5000 photons. There was little fluctuation across the lifetime duration of the molecule, with triplet lifetimes between 150 and 200 μs . A similar lack of variation in triplet lifetime over time was seen in all the molecules studied under ambient atmosphere, with the triplet lifetimes falling in the range of 100–300 μs and yields of 1–2%. These values are of a similar magnitude to that of other cNDIs;^[44] however, the triplet yield is slightly increased, suggesting there is a small HAE from the F atoms, but not sufficient to lead to significant increases in the ISC rate constant and yield. The triplet lifetime of **4** increased to 500–600 μs when measured under N_2 (Figure S17 in the Supporting Information), yet triplet yields remained at ~ 1 –2%, confirming triplet formation as the origin of these short-lived intermittencies. Despite the introduction of fluorine atoms, the triplet yield remains quite low and with short, sub-millisecond lifetimes, ensuring a constant fluorescent output from single molecules. These properties point to the suitability of these cNDIs for use in single-molecule labelling applications.

Conclusion

The synthesis and structural characterisation of two new fluorinated cNDIs have been presented and a comprehensive investigation into their optical properties in bulk solution and at the single-molecule level has been conducted. Both compounds show high quantum yields (~ 0.8) and long single-exponential fluorescence lifetimes (~ 13 ns) in a range solvents; values unprecedented in cNDIs. As single molecules, the compound with fluorinated core side chains showed excellent photon-emission properties with consistent photon output over $\sim 10^7$ – 10^8 cycles of excitation and emission. Interruptions or blinks in the photon stream lasting longer than milliseconds were exceptionally rare and shorter intermittencies due to triplet-state formation were also infrequent and had durations of ~ 100 ms in ambient conditions and yields of only 1–2%. These properties arise from fluorination of the core substituents, which is contrary to a common perception about heavy atom quenching effects and shows that fluorination can, in the right circumstances, lead to improved optical properties and an increase in molecular brightness without a significant increase in intersystem crossing yield. The high photostability and consistent photon emission from single molecules demonstrates that these compounds have high potential for single-molecule imaging and labelling applications.

Experimental Section

Materials

1,4,5,8-Naphthalenetetracarboxylic dianhydride and 1-hexanamine were obtained from Sigma–Aldrich and 2,2,3,3,4,4,5,5,6,6,6-undecafluorohexan-1-amine was purchased from Tokyo Chemical Industry (TCI). All chemicals were used as received. 2,6-Dibromo-naphthalene dianhydride was prepared following established literature pro-

cedures.^[18] Acetone, acetic acid, ethanol, dichloromethane, and dimethylformamide (DMF) were purchased from commercial suppliers. Benzonitrile, DMF, toluene and poly(methyl methacrylate) (PMMA) used for spectroscopic analysis were of the highest purity available from Aldrich or Merck.

Characterisation

Low-resolution electron-impact mass spectrometry (LR-MS) was performed on a Micromass Platform II API quadrupole electrospray mass spectrometer. High-resolution electron-impact mass spectrometry (HR-ESI) was performed on an Agilent Technologies 6220 Accurate-Mass Time-of-Flight LC/MS. 1H and ^{13}C NMR spectra were recorded by using a Bruker DRX 400 MHz NMR spectrometer (400 MHz for 1H NMR, 100 MHz for ^{13}C NMR) and a Bruker AV 600 MHz NMR spectrometer (600 MHz for 1H NMR, 150 MHz for ^{13}C NMR), using $CDCl_3$ unless otherwise stated. Chemical shifts are reported relative to the resonances of residual $CHCl_3$ at $\delta = 7.26$ ppm (H) and $\delta = 77.2$ ppm (C). Fluorine NMR spectra were recorded on a Bruker AV400 spectrometer at 400 MHz using $CFCl_3$ as the external reference at $\delta = 0$ ppm. NMR spectra for **2**–**5** are given in the Supporting Information, Figures S1–S11.

Synthesis

Synthesis of 4: *N,N'*-Bis(*n*-hexyl)-2,6-dibromo-1,4,5,8-naphthalenetetracarboxy diimide (**2**) (see the Supporting Information) (50 mg, 0.08 mmol), 2,2,3,3,4,4,5,5,6,6,6-undecafluorohexan-1-amine (0.10 g, 0.34 mmol), tris(dibenzylideneacetone)dipalladium(0) (2.3 mg, 2.53 μmol), 1,1'-bis(diphenylphosphine)ferrocene (0.5 mg, 0.84 μmol) and sodium *tert*-butoxide (9.7 mg, 1.08 mmol) were heated in dry toluene (50 mL) at 90 °C for 12 h. After this period, the reaction was cooled and the solvent removed under reduced pressure. The crude material was dissolved in 20% *n*-hexane in CH_2Cl_2 (50 mL) and passed through a pad of silica gel. The filtrate was concentrated and purified by column chromatography (20% *n*-hexane in CH_2Cl_2) to give the title compound **4** as a bright-pink solid (43 mg, 50%). M.p. > 200 °C; 1H NMR (400 MHz): $\delta = 9.88$ (t, $J = 6.8$ Hz, 2H, NH), 8.20 (s, 2H, NDI), 4.31–4.23 (m, 4H, NCH_2CF_2), 4.18 (dd, $J = 7.6, 7.6$ Hz, 4H, NCH_2), 1.76–1.68 (m, 4H, CH_2), 1.45–1.31 (m, 12H, CH_2), 0.90 ppm (t, $J = 6.8$ Hz, 6H, CH_3); ^{19}F NMR (400 MHz): $\delta = -80.72$ – -80.77 (m, 6F), -117.32 – -117.40 (m, 4F), -122.58 – -122.60 (m, 4F), -122.61 – -122.16 (m, 4F), -126.09 – -126.17 ppm (m, 4F); ^{13}C NMR (100 MHz, partial): $\delta = 166.4, 162.5, 149.0, 126.3, 121.8, 118.1, 104.0, 43.1, 40.9, 31.6, 28.1, 27.0, 22.7, 14.1$ ppm; HRMS (TQ-MS-ESI): m/z calcd for $C_{35}H_{38}F_{22}N_4O_4$: 1029.2302 [$M + H$]⁺; found: 1029.2312 [$M + H$]⁺.

Synthesis of 3: 2,2,3,3,4,4,5,5,6,6,6-Undecafluorohexan-1-amine (1.05 g, 3.52 mmol) was added to a suspension of 2,6-dibromo-1,4,5,8-naphthalenetetracarboxylic dianhydride (**1**) (0.50 g, 1.17 mmol) in acetic acid (80 mL), and the reaction heated at 130 °C for 4 h. The formed precipitate was filtered and recrystallised with CH_2Cl_2 /methanol to give the title compound as a pale-orange powder **3** (0.32 g, 28%). The compound was found to be rather insoluble in many organic solvents. M.p. > 250 °C; 1H NMR (400 MHz, $[D_6]DMSO$): $\delta = 9.43$ (s, 2H, NDI), 5.56 ppm (t, $J = 16.0$ Hz, 4H, NCH_2); ^{19}F NMR (400 MHz, $[D_6]DMSO$): $\delta = -80.72$ – -80.77 (m, 3F), -114.38 – -114.46 (m, 2F), -122.18 – -122.23 (m, 2F), -123.23 – -123.37 (m, 2F), -125.87 – -125.94 ppm (m, 2F); ^{13}C NMR (150 MHz, partial, $[D_6]DMSO$): $\delta = 155.7, 134.6, 128.8, 124.9$ ppm; HRMS (TQ-MS-ESI): m/z calcd for $C_{26}H_6Br_2N_2F_{22}O_4$: 987.8323 [M][−]; found: 987.8335 [M][−].

Synthesis of 5: *N,N'*-Bis(2,2,3,3,4,4,5,5,6,6,6-undecafluorohexyl)-2,6-dibromo-1,4,5,8-naphthalenetetracarboxy diimide (**3**) (50 mg,

0.05 mmol), 2,2,3,3,4,4,5,5,6,6,6-undecafluorohexan-1-amine (60 mg, 0.20 mmol), tris(dibenzylideneacetone)dipalladium(0) (1.4 mg, 1.52 μ mol), 1,1'-bis(diphenylphosphine)ferrocene (0.06 mg, 0.51 μ mol) and sodium *tert*-butoxide (2.8 mg, 0.05 mmol) were heated in dry toluene (50 mL) at 90 °C for 12 h. After this period, the reaction was cooled and the solvent removed under reduced pressure. The crude material was dissolved in 20% *n*-hexane in CH₂Cl₂ (50 mL) and passed through a pad of silica gel. The filtrate was concentrated and purified by column chromatography (20% *n*-hexane in CH₂Cl₂) to give the title compound **5** as a bright-pink solid (20 mg, 28%). M.p. > 200 °C; ¹H NMR (400 MHz): δ = 9.75 (br t, 2H, NH), 8.33 (s, 2H, NDI), 5.07–4.50 (br t, 4H, NCH₂CF₂), 4.30 ppm (br t, 4H, NCH₂); ¹⁹F NMR (400 MHz): δ = –80.74––80.79 (m, 12F), –114.84––114.90 (m, 4F), –117.14––117.21 (m, 4F), –122.56––122.59 (m, 8F), –123.10––123.13 (m, 4F), –123.63––126.65 (m, 4F), –126.16––126.18 ppm (m, 8F); ¹³C NMR (100 MHz, partial): δ = 165.5, 162.3, 149.5, 126.1, 122.2, 119.1, 103.7, 43.4, 38.7 ppm; HRMS (TQ-MS-ESI): *m/z* calcd for C₃₈H₁₁F₄₄N₄O₄: 1423.0078 [M–H][–]; found: 1423.0088 [M–H][–].

Electrochemical Methods

Electrochemical experiments were carried out in a standard three-electrode arrangement with a Bioanalytical Systems BAS Model 100B electrochemical workstation (Bioanalytical Systems, West Lafayette, IN, USA). A Pt wire was used as the auxiliary electrode, while another Pt wire in a frit (CH₂Cl₂, 0.1 M [Bu₄N][PF₆]) separated from bulk solution was used as a quasi-reference electrode. The potentials are quoted relative to the ferrocene/ferrocenium (Fc/Fc⁺) potential scale, as an internal reference. A glassy carbon (GC) working electrode (ALS, Japan) with a diameter (*d* = 0.10 cm) was used for cyclic voltammetry experiments. Prior to each voltammetry experiment, the working electrode was polished with 0.3 μ m alumina on a clean polishing cloth (Buehler, USA), rinsed with water, then acetone and finally dried under nitrogen gas. The solutions used for voltammetry measurements were purged with solvent-saturated nitrogen gas prior to commencement of an experiment and blanketed with nitrogen during the course of the experiment. All voltammetry studies were carried out at room temperature (20 ± 2 °C). The supporting electrolyte [Bu₄N][PF₆] (GFS Chemicals, 98%) was recrystallised twice from ethanol.^[45]

Spectroscopic Methods

Absorbance spectra were run on a Varian model Cary 60 UV/Visible spectrophotometer in 1 cm quartz cuvettes. Steady-state fluorescence measurements were taken on a Varian model Cary Eclipse fluorescence spectrophotometer with intensity corrected for detector efficiency. Fluorescence quantum yields of compounds **4** and **5** were determined by using the comparative method with Rhodamine 6G (Φ_f = 0.95 in ethanol)^[46] as the reference standard. Solutions were prepared in 1 cm quartz cuvettes, with absorbance maxima less than 0.10 in order to prevent inner filter effects. Samples were deoxygenated by bubbling with N₂ for 20 min immediately prior to measurement of fluorescence emission spectra. Time-resolved fluorescence decays were measured on a previously described home-built set-up.^[20] Briefly, excitation was provided by the supercontinuum fiber laser described below, emission passed through a monochromator (CVI, dk480) and detected by an avalanche photodiode (APD: Id-Quantique, Id-100). Photon timing was achieved by using the PicoQuant hardware and software described below. Data were fit by an exponential decay convolved with the instrument response function (IRF) recorded from light scattered by a solution of milk powder in water (IRF typically ~90–100 ps,

FWHM). Goodness-of-fit of the data by the fitting function was determined by the χ^2 fitting parameter and the distribution of the fit residuals.

Single-molecule samples of **1** were prepared by serial dilution into 1% solution of PMMA until a final concentration of ~10^{–10} M. Samples were spin-cast onto thoroughly cleaned glass cover slips at 2000 rpm for 60 s, yielding a film thickness of ~100–200 nm. Wide-field imaging was achieved by using a previously described set up,^[47] equipped with a 100× 1.3 N.A. oil immersion objective (Olympus). Confocal microscopy measurements were performed by using a pulse-picked supercontinuum fiber laser (Fianium, SC 400–4-pp) with pulses of ~40 ps across the visible and near-IR range. The excitation wavelength was selected by using a 10 nm band pass filter (Chroma). The light was then passed through a focusing lens through a 10 μ m pinhole (Thorlabs) and then collimated. The light was directed through an inverted Olympus IX71 microscope and focused onto the sample using a 100× 1.4 N.A. oil immersion objective (Olympus). Emission from the sample was collected through the same objective, separated from excitation light by a dichroic mirror (Chroma), passed through a long pass filter (Chroma) and was either sent directly though to an avalanche photodiode (APD, PicoQuant, τ -SPAD) or was split using a 50:50 beamsplitting prism (Edmund Optics) between the APD and through a spectrograph (Princeton Instruments) to an EMCCD camera (Princeton Instruments, ProEM512). Molecules were selected by scanning a 10× 10 μ m area by using a Piezo stage (Physik Instrumente, P-733.2CL) and controller (Physik Instrumente, E-710). Emission times were recorded by using a photon counting device (Picoquant, PicoHarp 300) through a router (Picoquant, PHR 800) with a trigger diode assembly (PicoQuant, TDA 200) to provide the start signal. Data collection was performed by using the SymPhoTime (Picoquant) and WinSpec (Princeton) software suites. The photon stream from the APD was collected in t3r mode where both macro times (time from start of measurement) and micro times (time from previous laser pulse) were recorded for every photon. Single-molecule trajectories (from macro times) and decay profiles (from micro times) were constructed and analysed by using the BIFL software package (Scientific Software Technologies Center). Single-molecule decay profiles were fit by an exponential decay convolved with an IRF recorded from excitation light scattered by a blank coverslip (IRF typically ~700–800 ps, FWHM for the confocal set-up). Goodness-of-fit of the data by the fitting function was determined by the reduced χ^2 fitting parameter returned by the BIFL software and the distribution of the fit residuals.

Supporting Information available: Synthesis of **2**, NMR spectra for **2–5**, electrochemical data for **4** and **5**, X-ray crystallography data for **5**, molar absorption coefficients for **4** and **5**, optical spectra for **4** and **5**, time-resolved fluorescence data and calculation of radiative and non-radiative rate constants, triplet lifetimes of single molecules of **4**.

Acknowledgements

Financial support from the Australian Research Council through the Discovery Grant Scheme (DP130101861) is gratefully acknowledged. We thank Craig Forsyth for technical assistance with X-ray crystallography.

Keywords: fluorescence quantum yield • naphthalene diimide • photostability • single-molecule studies • time-resolved spectroscopy

- [1] H. Brinkmann, C. Kelting, S. Makarov, O. Tsaryova, G. Schnurpfeil, D. Woehrle, D. Schlettwein, *Phys. Status Solidi A* **2008**, *205*, 409–420.
- [2] F. Babudri, G. M. Farinola, F. Naso, R. Ragni, *Chem. Commun.* **2007**, 1003–1022.
- [3] T. Okamoto, K. Nakahara, A. Saeki, S. Seki, J. H. Oh, H. B. Akkerman, Z. Bao, Y. Matsuo, *Chem. Mater.* **2011**, *23*, 1646–1649.
- [4] M. Gliboff, H. Li, K. M. Knesting, A. J. Giordano, D. Nordlund, G. T. Seidler, J.-L. Bredas, S. R. Marder, D. S. Ginger, *J. Phys. Chem. C* **2013**, *117*, 15139–15147.
- [5] M. G. Dhara, S. Banerjee, *Prog. Polym. Sci.* **2010**, *35*, 1022–1077.
- [6] J. A. Gladysz, M. Jurisch, *Top. Curr. Chem.* **2012**, *308*, 1–24.
- [7] M.-L. Tang, Z.-N. Bao, *Chem. Mater.* **2011**, *23*, 446–455.
- [8] S. Maniam, A. B. Holmes, J. Krstina, G. A. Leeke, G. E. Collis, *Green Chem.* **2011**, *13*, 3329–3332.
- [9] H. E. Katz, A. J. Lovinger, J. Johnson, C. Kloc, T. Siegrist, W. Li, Y. Y. Lin, A. Dodabalapur, *Nature* **2000**, *404*, 478–481.
- [10] A. R. Gutierrez, D. G. Whitten, *J. Am. Chem. Soc.* **1974**, *96*, 7128–7130.
- [11] T. C. Werner, *Fluoresc. News* **1976**, *9*, 1–4.
- [12] M. Rae, F. Perez-Balderas, C. Baleizao, A. Fedorov, J. A. S. Cavaleiro, A. C. Tome, M. N. Berberan-Santos, *J. Phys. Chem. B* **2006**, *110*, 12809–12814.
- [13] D. F. Eaton, *J. Am. Chem. Soc.* **1981**, *103*, 7235–7239.
- [14] F. Würthner, S. Ahmed, C. Thalacker, T. Debaerdemaeker, *Chem. Eur. J.* **2002**, *8*, 4742–4750.
- [15] M. A. H. Alamiry, A. C. Benniston, J. Hagon, T. P. L. Winstanley, H. Lemmetyinen, N. V. Tkachenko, *RSC Adv.* **2012**, *2*, 4944–4950.
- [16] D. Yan, D.-K. Bucar, A. Delori, B. Patel, G. O. Lloyd, W. Jones, X. Duan, *Chem. Eur. J.* **2013**, *19*, 8213–8219.
- [17] C.-L. Sun, J. Li, H.-W. Geng, H. Li, Y. Ai, Q. Wang, S.-L. Pan, H.-L. Zhang, *Chem. Asian J.* **2013**, *8*, 3091–3100.
- [18] T. D. M. Bell, S. Yap, C. H. Jani, S. V. Bhosale, J. Hofkens, F. C. De Schryver, S. J. Langford, K. P. Ghiggino, *Chem. Asian J.* **2009**, *4*, 1542–1550.
- [19] H. F. Higginbotham, S. Maniam, S. J. Langford, T. D. M. Bell, *Dyes Pigm.* **2015**, *112*, 290–297.
- [20] R. P. Cox, H. F. Higginbotham, B. A. Graystone, S. Sandanayake, S. J. Langford, T. D. M. Bell, *Chem. Phys. Lett.* **2012**, *521*, 59–63.
- [21] H. F. Higginbotham, R. P. Cox, S. Sandanayake, B. A. Graystone, S. J. Langford, T. D. M. Bell, *Chem. Commun.* **2013**, *49*, 5061–5063.
- [22] S. V. Bhosale, C. H. Jani, C. H. Lalander, S. J. Langford, I. Nerush, J. G. Shapter, D. Villamaina, E. Vauthey, *Chem. Commun.* **2011**, *47*, 8226–8228.
- [23] K. A. Lee, V. Lozan, S. J. Langford, B. Kersting, *Dalton Trans.* **2009**, 7481–7485.
- [24] K. A. Willets, O. Ostroverkhova, M. He, R. J. Twieg, W. E. Moerner, *J. Am. Chem. Soc.* **2003**, *125*, 1174–1175.
- [25] W. E. Moerner, *J. Phys. Chem. B* **2002**, *106*, 910–927.
- [26] S. V. Bhosale, C. H. Jani, S. J. Langford, *Chem. Soc. Rev.* **2008**, *37*, 331–342.
- [27] N. Sakai, J. Mareda, E. Vauthey, S. Matile, *Chem. Commun.* **2010**, *46*, 4225–4237.
- [28] S.-L. Suraru, F. Würthner, *Angew. Chem. Int. Ed.* **2014**, *53*, 7428–7448; *Angew. Chem.* **2014**, *126*, 7558–7578.
- [29] T. He, M. Stolte, F. Würthner, *Adv. Mater.* **2013**, *25*, 6951–6955.
- [30] M. Stolte, S. L. Suraru, F. Würthner, J. H. Oh, Z. Bao, J. Brill, M. Köne-mann, J. Qu, U. Zschieschang, H. Klauck, *Proc. of SPIE* **2010**, *7778*, 777801–777808.
- [31] B. J. Jung, J. Sun, T. Lee, A. Sarjeant, H. E. Katz, *Chem. Mater.* **2009**, *21*, 94–101.
- [32] H. E. Katz, J. Johnson, A. J. Lovinger, W. Li, *J. Am. Chem. Soc.* **2000**, *122*, 7787–7792.
- [33] B. A. Jones, A. Facchetti, T. J. Marks, M. R. Wasielewski, *Chem. Mater.* **2007**, *19*, 2703–2705.
- [34] Z. Yuan, J. Li, Y. Xiao, Z. Li, X. Qian, *J. Org. Chem.* **2010**, *75*, 3007–3016.
- [35] Y. Li, C. Li, W. Yue, W. Jiang, R. Kopecek, J. Qu, Z. Wang, *Org. Lett.* **2010**, *12*, 2374–2377.
- [36] Crystal data for **5**: [C₄₁H₁₉F₄₄N₄O₄]; 0.25×0.12×0.05 mm³; a = 5.0868(9), b = 15.041(2), c = 16.0457(18) Å; α = 92°, β = 90°, γ = 98°; triclinic; P1; Z = 2, V = 1213.2(3) Å³, ρ_{calc} = 2.009 Mg m⁻³; F(000) = 721; λ = 0.71073 Å; T = 123(2) K; μ = 0.244 mm⁻¹; Nonius Kappa CCD diffractometer, φ and ω scan data, 10079 data collected, 5458 unique reflections (R_{int} = 0.0342) and 10079 observed [I > 2σ(I)], 437 refined parameters; R1 = 0.0486; Rw2 = 0.0950. Crystallographic data (excluding structure factors) for **5** have been deposited with the Cambridge Crystallographic Data Centre. CCDC 1026275 contains the supplementary crystallographic data for this paper. These data can be obtained free of charge from The Cambridge Crystallographic Data Centre via www.ccdc.cam.ac.uk/data_request/cif.
- [37] C. Röger, Y. Miloslavina, D. Brunner, A. R. Holzwarth, F. Würthner, *J. Am. Chem. Soc.* **2008**, *130*, 5929–5939.
- [38] F. Doria, I. Manet, V. Grande, S. Monti, M. Freccero, *J. Org. Chem.* **2013**, *78*, 8065–8073.
- [39] S. Guo, J. Sun, L. Ma, W. You, P. Yang, J. Zhao, *Dyes Pigm.* **2013**, *96*, 449–458.
- [40] Y. V. Suseela, M. Sasikumar, T. Govindaraju, *Tetrahedron Lett.* **2013**, *54*, 6314–6318.
- [41] M. Orrit, *Photochem. Photobiol. Sci.* **2010**, *9*, 637–642.
- [42] M. Haase, C. G. Huebner, F. Nolde, K. Müllen, T. Basche, *Phys. Chem. Chem. Phys.* **2011**, *13*, 1776–1785.
- [43] K. D. Weston, P. J. Carson, H. Metiu, S. K. Buratto, *J. Chem. Phys.* **1998**, *109*, 7474–7485.
- [44] T. D. M. Bell, S. Yap, C. Jani, S. J. Langford, J. Hofkens, F. De Schryver, K. P. Ghiggino, *Proc. of SPIE* **2007**, *6444*, 644404–1.
- [45] *Electrochemistry for Chemists*, 2nd ed. (Eds.: D. T. Sawyer, A. Sobkowiak, J. J. L. Roberts) Wiley, Hoboken, **1995**.
- [46] R. F. Kubin, A. N. Fletcher, *J. Lumin.* **1982**, *27*, 455–462.
- [47] D. R. Whelan, T. Holm, M. Sauer, T. D. M. Bell, *Aust. J. Chem.* **2014**, *67*, 179–183.

Received: October 29, 2014

Published online on January 29, 2015